Modeling Mass Transfer and Hydrodynamics in Fluidized-Bed Adsorption of Proteins

Pamela R. Wright and Benjamin J. Glasser
Dept. of Chemical and Biochemical Engineering, Rutgers University, Piscataway, NJ 08854

A model was developed and solved to describe protein adsorption in a fluidized bed. Liquid-solid mass transfer, adsorption and hydrodynamic effects were taken into account. The model was examined for both pore and homogeneous diffusion. The simulation results showed close agreement with experimental breakthrough curves obtained for lysozyme adsorption on Streamline SP and S-HyperD LS resins at expansions of 2, 3 and 4 times the settled-bed height. Parametric sensitivity analysis showed that superficial velocity and particle radius had the largest effects on breakthrough behavior for all conditions. The effect of axial dispersion, film mass transfer and solid diffusion coefficients were less significant contributors to breakthrough at all expansions and bulk phase viscosities. The simulation results for pore diffusion were affected more significantly by changes in superficial velocity and particle radius than the simulation results for homogeneous diffusion. The performance of the fluidized-bed adsorption unit was limited by intraparticle mass-transfer effects, especially at high degrees of bed expansion.

Introduction

Solid-liquid fluidized-bed systems have been used for many applications in the chemical and biochemical industries. Recently this technology has been applied as a downstream processing technique in the pharmaceutical industries for the primary recovery of therapeutic proteins from mammalian cell culture, yeast, and *E. coli* fermentation feedstocks (Draeger and Chase, 1990, 1991; Bailey et al., 1998; Thommes, 1997). Fluidized- or expanded-bed adsorption is a single-pass unit operation in which proteins are recovered and concentrated from crude feedstock and transferred to a process for chromatographic purification, without the need for feedstock clarification. (Thommes (1997) and Karau et al. (1997) have defined expanded-bed adsorption as a subset of fluidized-bed adsorption that specifically addresses situations with low superficial velocities close to the minimum fluidization velocity. For most resins the expression "expanded-bed adsorption" is applicable only to bed expansions of less than two times the settled bed height. In this article adsorption was investigated at bed expansions of two to four times the settled bed height. Thus, we have used the expression "fluidized-bed adsorption" to emphasize that we are investigating protein adsorption for a large range of bed expansions, including high expansions.)

Correspondence concerning this article should be addressed to B. J. Glasser.

Although this unit operation offers many economically attractive advantages over conventional primary recovery methods, process times can be very long and currently there is not a good way to predict, *a priori*, adsorption performance in a fluidized-bed adsorption system. Therefore, a predictive model that could provide a fundamental understanding of adsorption as a function of bed expansion hydrodynamics would be extremely useful and could lead to advances in the optimization of this technology. Such an understanding would facilitate both the selection of appropriate chromatographic media and the operating conditions for a particular application (to increase throughput without compromising product recovery).

Fluidized-bed adsorption has been studied both experimentally and theoretically for liquid–solid systems. Chung and Wen (1963) were among the first to model dispersion in a liquid–solid fluidized bed using water and glass beads over a wide range of Reynolds numbers. It was found that fluid velocity has a strong effect on the axial dispersion coefficient in fluidized beds. Later, Fan et al. (1964) developed correlations for overall mass transfer in a fluidized bed as a function of Reynolds number. Most modeling work developed subsequently has focused on hydrodynamic factors associated with superficial velocity, bed expansion, and axial dispersion

(Foscolo and Gibilaro, 1984; Johansson and Wnukowski, 1992; Poncelet et al., 1990). These models are in good agreement with the correlation of Richardson and Zaki (1954) for particle fluidization for a wide range of expansions and bulk-phase viscosities, but the issue of adsorption was not addressed.

More recent work has been carried out to address dynamic behavior in fluidized beds (Kaufman et al., 1995; Thelen and Ramirez, 1997; Thelen and Ramirez, 1999). These models take a more detailed approach to hydrodynamic modeling to include transient disturbances during adsorption that may lead to limitations in biological applications of fluidized-bed adsorption systems. Performance of expanded-bed adsorption systems for protein separation has been assumed to be limited by hydrodynamic effects, since adsorption capacity and breakthrough times usually decrease at high degrees of bed expansion and increased axial dispersion (Chang and Chase, 1996). However, it is extremely difficult to experimentally uncouple mass-transfer effects from hydrodynamic effects to understand mechanistic limitations, since these effects are interdependent. As a result, the significance of intraparticle mass-transfer effects in expanded-bed adsorption is implied, but mass-transfer effects have not been modeled or quantified in terms of other mechanistic features for a range of operating conditions.

Veeraraghavan and Fan (1989) developed a simulation to model adsorption in a liquid–solid fluidized bed using granular activated carbon to adsorb phenol from an aqueous feedstock. The model accounted for axial dispersion and mass-transfer effects, and identified the dominant mechanistic features of phenol adsorption based on a homogeneous diffusion model for mass uptake in the solid particles. Some deviations between experimental and simulated results were observed and were attributed to the application of a homogeneous diffusion model to a pore-diffusion adsorption mechanism. From the parametric sensitivity analysis, it was concluded that since the experiments were conducted under conditions that were not sensitive to changes in axial dispersion, the simulation could not be used to isolate axial dispersion effects.

It is often assumed that axial dispersion may be negligible in a long column (Bascoul et al., 1988; Thommes et al., 1995). In a fluidized-bed adsorption system, however, it is important to examine the magnitude of axial dispersion relative to other effects. The validity of assuming that axial dispersion is negligible relative to other effects such as intraparticle mass transfer and superficial velocity has not been confirmed. Furthermore, most models and simulations have only considered a small operating range using only one particle mass-transfer mechanism. To obtain a fundamental understanding of expanded-bed adsorption, the interdependence of these parameters over a wide range of bed expansions and bulk-phase viscosities needs to be considered in terms of the different possible mass-transfer mechanisms.

The objective of this work was to simulate fluidized-bed adsorption by taking into account mass transfer, hydrodynamics, and adsorption. The effectiveness of the modeling effort was ascertained by comparing the results to lysozyme adsorption in a fluidized-bed system for various operating conditions. The comparison was made for lysozyme adsorption on two commercially available resins. The first, Streamline SP, is a macroporous resin, and mass transfer in the resin was simulated using a pore-diffusion model. The second, S-HyperD LS, is a gel composite resin, and mass transfer in the resin was simulated using a homogeneous-diffusion model. The axial dispersion coefficient and effective solid-diffusion coefficients were experimentally obtained from tracer studies and batch adsorption data, respectively. Other parameters, such as the film mass-transfer coefficient, expanded-bed void fraction, and solid-dispersion coefficient, were obtained from well-established correlations calculated for each bed expansion and fluid viscosity. Our results show that such a model can be used to predict, *a priori*, breakthrough and adsorption performance as a function of expanded-bed height, from batch adsorption data and data obtained from tracer studies (at the desired bulk-phase viscosity). Finally, a parametric sensitivity analysis was carried out to isolate axial dispersion effects from mass-transfer effects as a function of the solid-phase mass-transfer mechanism and bed expansion.

Model Development

In the model development for both pore diffusion and solid diffusion, several assumptions have been made. These assumptions have been made in order to arrive at a model that can simply yet accurately describe the important physical processes in the column. These assumptions are as follows [see Wright (2000) for further details]: (1) resin particles are monosize and the average particle size is used for both Streamline SP and S-HyperD LS; (2) radial concentration gradients in the column are negligible relative to axial concentration gradients; (3) adsorption is well represented by a Langmuir isotherm for both Streamline SP and S-HyperD LS resins; (4) adsorption at the surface of the particle is instantaneous with local equilibrium at the particle surface; (5) hydrodynamic behavior can be described by the axial dispersion model; (6) a constantly changing boundary at the particle surface is applied until equilibrium is attained; (7) mass transfer in the particles can be modeled using batch uptake data for pore and solid diffusion.

Derivation of Model Equations

In this work mass-transfer effects for homogeneous diffusion and pore diffusion were modeled to assess the impact of the mass-transfer mechanism and intraparticle mass-transfer resistance as functions of hydrodynamic factors. Mass-transfer effects were modeled and validated against experimental breakthrough data for S-HyperD LS and Streamline SP cation exchange resins.

Mass Balances for a Fluidized Bed. Following Veeraraghavan and Fan (1989), the mass balance with respect to liquid and solid phases for a segment of the column between z and $z + \Delta z$ is:

Accumulation in the liquid + mass in $|_{\text{bulk flow}}$
+ mass in $|_{\text{dispersion}}$ = mass out $|_{\text{bulk flow}}$
+ mass out $|_{\text{dispersion}}$ − mass transfer to the solid.

The resulting mass balance for the liquid side is then

$$\epsilon_L \frac{\partial C}{\partial t} = D_{\text{ax}} \epsilon_L \frac{\partial^2 C}{\partial z^2} - u \epsilon_L \frac{\partial C}{\partial z} - \frac{3 k_f \epsilon_s (C - C_f)}{R}, \quad (1)$$

where C is the bulk-phase concentration of protein, $\epsilon_s = V_m/V$ is the volume fraction of solids (or resin), V_m is the volume of resin in the column, V is the volume of the expanded bed, ϵ_L is the liquid void fraction in the expanded bed given by McCabe et al. (1985), and ϵ_o is the settled bed void fraction. The axial dispersion coefficient, D_{ax}, was determined experimentally by tracer studies for each condition (Wright et al., 1999). We will assume that the superficial velocity, u, is a constant throughout the bed, which is a good approximation for low protein concentrations and an incompressible fluid. The reason for making use of an experimentally determined axial dispersion coefficient is that our understanding of the micromechanics of fluidized beds is not yet at a point where axial dispersion coefficients can be predicted *a priori*. Equation 1 is solved using the following initial and boundary conditions:

$$\text{I.C.:} \quad \text{at } t = 0,\ C(z,0) = 0 \quad \text{for} \quad 0 \le z \le H \tag{1a}$$

$$\text{B.C.1:} \quad \text{at } z = 0,\ C - \frac{D_{ax}\epsilon_L}{u}\frac{\partial C}{\partial z} = Co \quad \text{for} \quad t > 0 \tag{1b}$$

$$\text{B.C.2:} \quad \text{at } z = H,\ \frac{\partial C}{\partial z} = 0 \quad \text{for} \quad t > 0 \tag{1c}$$

Since the particles are fluidized with a buffer before the feedstock is introduced, the initial condition (Eq. 1a) mathematically represents the fact that initially there is no protein concentration in the column. Boundary condition 1 relates the effects of axial dispersion to the feed concentration of protein. Boundary condition 2 implies that at the top of the column, where there are no more resin particles, there is no change in concentration.

In the solid phase, dispersion is still accounted for in terms of the amount of protein adsorbed, and so the mass balance is described as

$$\text{Accumulation} = \text{mass in}\,|_{\text{dispersion}} - \text{mass out}\,|_{\text{dispersion}} + \text{mass transfer to the solid,}$$

which is written as:

$$\epsilon_s\frac{\partial q'}{\partial t} = D_s\frac{\partial^2 q'}{\partial z^2} + \frac{3k_f\epsilon_s(C - C_f)}{R}, \tag{2}$$

where q' is the average solid-phase concentration at a given height. Since there are no experimental data available for solids mixing for the particles of interest in a fluidized bed, values for the solid dispersion term, D_s, were obtained by the correlation of Van Der Meer et al. (1984), using experimental values for superficial velocity, u, at each expansion:

$$D_s = 0.04u^{1.8}\ \text{m}^2/\text{s}, \tag{3}$$

where the constant 0.04 is dimensional. Although other correlations for solid dispersion exist, the correlation of Van Der Meer et al. is most appropriate for the frontal adsorption application described here, since the correlation was developed using dispersion measurements between two fractions of differing particle size. For protein adsorption, Thommes (1997) has reported that values of solid dispersion are expected to be less than 10% of the axial dispersion. Solid-dispersion values calculated from Eq. 3 for all cases considered in this article are less than 10% of the corresponding measured axial dispersion value. It should be noted that if we set D_s equal to zero, then we recover the mass balance for the solid phase corresponding to a packed bed (or a fluidized bed with negligible solid dispersion).

The film mass-transfer coefficient, k_f, was calculated for expanded-bed adsorption as a function of bed void fraction using the correlation of Fan et al. (1960):

$$k_f = \frac{D_m}{d_p}\left[2 + \left(1.5(1-\epsilon_L)Re_p^{1/2}Sc^{1/3}\right)\right], \tag{4}$$

where Re_p is the particle Reynolds number, Sc is the Schmidt number, and D_m is the molecular diffusion coefficient of lysozyme in the fluid. While many correlations for k_f exist for packed- and fluidized-bed applications, direct measurements of k_f do not exist for expanded-bed adsorption systems. The correlation of Fan et al. (1960) was used in the simulation presented here since the values for k_f obtained from this correlation were in close agreement with data obtained by the batch simulation of both S-HyperD and Streamline SP in 30% glycerol solutions where film mass-transfer effects are most significant (Wright et al., 1998). As expected, k_f increases gradually with increases in linear velocity using Eq. 4. Furthermore, this correlation accounts for changes in film mass transfer as a function of bed voidage and solution viscosity without the need for assumed proportionality constants that may be system specific (Rowe, 1975).

Equation 2 is solved using the following initial and boundary conditions:

$$\text{I.C.:} \quad \text{at } t = 0,\ q'(z,0) = 0 \quad \text{for} \quad 0 \le z \le H \tag{2a}$$

$$\text{B.C.1:} \quad \text{at } z = 0,\ \frac{\partial q'}{\partial z} = 0 \quad \text{for } t > 0 \tag{2b}$$

$$\text{B.C.2:} \quad \text{at } z = H,\ \frac{\partial q'}{\partial z} = 0 \quad \text{for } t > 0. \tag{2c}$$

In Eq. 2 and the subsequent boundary conditions q' represents the average solid-phase concentration as a function of z for each time interval. Initially, there is no protein in the column so there is no change in the average solid concentration. Similarly, we assume that where there are no particles, no adsorption can occur and boundary conditions 1 and 2 mathematically describe this assumption. Equations 1 and 2 are partial differential equations in z and t, and describe mass transfer in a fluidized bed with a constant superficial velocity. In order to account for mass transfer and adsorption in the resin particles, we need to write mass balances for the particles themselves and relate these mass balances to the preceding equations. This will be accomplished by recognizing that any change in the average solid-phase concentration q' will arise due to material diffusing into the particle at its surface.

One of the most critical aspects of fluidized-bed adsorption is resin selection. Porous gel-filled particles, such as S-HyperD LS, lead to the physical situation whereby adsorbed proteins move between charges in the gel. The migration

through the particle is random and driven solely by solid diffusion. Since there are no pores in the particle, a homogeneous diffusion model is appropriate to describe diffusion in the particle. In contrast for a porous particle like Streamline SP it is appropriate to model diffusion using a pore-diffusion model (Hall et al., 1966; Suzuki and Kawazoe, 1975; Slater, 1992; Weaver and Carta, 1996) that takes into account both solid diffusion (adsorbed protein) as well as pore diffusion (of the protein in the liquid in the pores). For this reason, we have presented equations to describe both homogeneous and pore diffusion and investigated how the different diffusional processes can affect fluidized-bed adsorption. Below, we first present equations for homogeneous diffusion, and this is followed by a presentation of equations for pore diffusion.

Homogeneous Diffusion in a Fluidized Bed. The governing equation for homogeneous diffusion is written as (Suzuki et al., 1975):

$$\frac{\partial q}{\partial t} = D\frac{1}{r^2}\frac{\partial}{\partial r}\left(r^2\frac{\partial q}{\partial r}\right), \tag{5}$$

where q is the total protein concentration in the solid phase (that is, in a resin particle). Equation 5 describes the change in solid-phase concentration in the particle as a function of time and particle radius (for a given axial position), and is solved using the following initial and boundary conditions:

$$\text{I.C.: at } t = 0,\ q\,(z,r,0) = 0 \qquad \text{for} \quad 0 \le z \le H \tag{5a}$$

$$\text{B.C.1: at} \quad r = 0,\ \frac{\partial q}{\partial r} = 0 \qquad \text{for} \quad t > 0 \tag{5b}$$

$$\text{B.C.2: at} \quad r = R,\ \frac{\partial q}{\partial r} = \frac{RD_s}{3D\epsilon_s}\frac{\partial^2 q'}{\partial z^2} + \frac{k_f(C - C_f)}{D} \qquad \text{for } t > 0. \tag{5c}$$

The initial condition describes the fact that the resin particles initially contain no protein. The first boundary condition describes the fact at the center of the particle we have symmetry. Physically the second boundary condition describes the fact that the increase in the solid-phase concentration can be attributed to the mass of protein that is transferred to a particle at its surface. This boundary condition is complicated by the fact that we have accounted for solid dispersion. Without solid dispersion, this boundary condition takes on the familiar form for a packed bed where the diffusional flux at the surface equals the external flux (that is, the film mass-transfer coefficient multiplied by the concentration difference). This form for the boundary condition is obtained by solving Eq. 2 for $(\partial q'/\partial t)$ and substituting the result into

$$\frac{\partial q}{\partial r} = \frac{R}{3D}\frac{\partial q'}{\partial t}.$$

Equation 5c mathematically relates changes in the solid-phase concentration to surface phenomena such as solid dispersion and film mass transfer as a function of axial position in the column. Therefore, both mass transfer and dispersive effects are taken into account in the solution of Eq. 5. Equation 5 represents a partial differential equation in r and t for a given axial position, z.

Experimental uptake data confirms that protein adsorption by S-HyperD LS is well represented by a Langmuir isotherm (Weaver and Carta, 1996; Wright et al., 1998). For this case, the following expression for the isotherm applies to homogeneous diffusion:

$$q = \frac{q_{\max}C}{K_s + C}. \tag{6}$$

Equation 5 and the associated boundary conditions are solved using orthogonal collocation. The solid-phase diffusion coefficient was obtained from simulation of experimental stirred cell batch uptake curves (Wright et al., 1998; Wright, 2000). In particular, we matched simulated uptake curves for lysozyme mass transfer and adsorption (in the resin particles) with experimental uptake curves. The diffusion coefficient was determined by examining conditions corresponding to a high Biot number where the intraparticle mass-transfer resistance dominated. The experiments and simulations were conducted for different resin loadings and bulk-phase viscosities. Since the uptake curves changed considerably with resin loading, but the diffusion coefficient should be independent of resin loading, these experiments were used to validate the applicability of such a procedure. In addition, by varying the resin loading we were able to study uptake rates where the particles never became saturated, as well as cases where the particles became completely saturated. Last, since the S-HyperD LS resin is filled with cross-linked gel, its diffusion coefficient should be independent of bulk-phase viscosity (which was indeed what we found). For S-HyperD LS, $D = 1.0 \pm 0.25 \times 10^{-8}$ cm^2/s for lysozyme adsorption by homogeneous diffusion under all conditions.

Pore Diffusion in a Fluidized Bed. In pore diffusion, Eqs. 1 and 2 apply in the same way as for homogeneous diffusion. However, mass uptake in the particle is governed by pore diffusion according to the following equation:

$$\frac{\partial q}{\partial t} = D\left[\frac{1}{r^2}\frac{\partial}{\partial r}\left(r^2\frac{\partial C_p}{\partial r}\right)\right], \tag{7}$$

where q is the total protein concentration in the solid phase represented by:

$$q = C_p + ma_pC_s. \tag{8}$$

In Eq. 8, C_p and C_s are the pore and solid (adsorbed) protein concentrations, respectively. Therefore, the total protein concentration in a macroporous particle consists of both the site bound (adsorbed) and pore concentrations. Experimental batch uptake data for lysozyme adsorption by a macroporous particle like Streamline SP are well represented by a Langmuir isotherm in accordance with the following equation (Pedersen et al., 1985; Weaver and Carta, 1996; Wright et al., 1998):

$$C_s = \frac{q_{\max}C_p}{K_s + C_p}. \tag{9}$$

Equation 7 is solved using the following initial and boundary conditions

$$\text{I.C.: at } t = 0,\ q(z,r,0) = 0 \tag{7a}$$

$$\text{B.C.1: at } r = 0,\ \frac{\partial C_p}{\partial r} = 0 \quad \text{for } t > 0 \tag{7b}$$

$$\text{B.C.2: at } r = R,\ \frac{\partial C_p}{\partial r} = \frac{RD_s}{3D\epsilon_s}\frac{\partial^2 q'}{\partial z^2} + \frac{k_f(C - C_p)}{D}. \tag{7c}$$

As in the previous section for homogeneous diffusion, the initial condition describes the fact that the resin particles initially contain no protein. The first boundary condition describes the fact that at the center of the particle we have symmetry. Physically, the second boundary condition describes the fact that the increase in the resin protein concentration can be attributed to the mass of protein that is transferred to a particle at its surface. Equation 7c was obtained by the following derivation

$$V_B\frac{\partial C}{\partial t} = -\epsilon_s D 4\pi R^2 \left.\frac{\partial C_p}{\partial r}\right|_{r=R}, \tag{10}$$

where

$$\left.\frac{\partial C_p}{\partial r}\right|_{r=R} = \frac{-k_f(C_p - C)}{\epsilon_s D}, \tag{11}$$

and thus,

$$\frac{\partial C}{\partial t} = \frac{V_m 3k_f(C - C_p)}{RV}. \tag{12}$$

The mass balance in the column (Eq. 2),

$$\epsilon_s\frac{\partial q'}{\partial t} = D_s\frac{\partial^2 q'}{\partial z^2} + \frac{3k_f\epsilon_s(C - C_p)}{R} \tag{13}$$

is then solved for $(\partial q'/\partial t)$, and the result is substituted into

$$\frac{\partial q}{\partial r} = \frac{R}{3D}\frac{\partial q'}{\partial t}.$$

The boundary conditions for pore diffusion relate changes in the pore concentration to solid dispersion and film mass-transfer effects as a function of position in the column. Once again, this boundary condition is complicated by the fact that we have accounted for solid dispersion; without solid dispersion this boundary condition takes on the familiar form for a packed bed where the diffusional flux at the surface equals the external flux. The solid-phase diffusion coefficient, D, was obtained from simulation of experimental stirred cell batch uptake curves (Wright et al., 1998; Wright, 2000). The same procedure as (discussed earlier) for S-HyperD LS was used for determining the diffusion coefficient. However, since the Streamline SP particles were porous (and therefore filled with the bulk fluid), we would expect that the effective solid diffusion coefficient should decrease with increases in bulk phase viscosity (which was what we found). For Streamline SP, $D = 3.5 \pm 0.5 \times 10^{-7}$cm^2/s for lysozyme adsorption by pore diffusion in the buffer. In 30% glycerol, the effective solid diffusion coefficient was determined to be $1.0 \pm 0.3 \times 10^{-7}$ cm^2/s for lysozyme adsorption.

Simulation

The column was modeled as a continuum of particles dispersed evenly in liquid for an expanded-bed height, H. Fluidized-bed heights of 20, 30, and 40 cm were investigated, taking into account the increase in bed porosity due to expansion. The resin loading was 100 mL for all cases, and the settled-bed height, H_o was fixed at 10 cm (to correspond to the experiments). The evolution of the liquid and solid concentrations as a function of time and axial position is described by Eqs. 1 and 2, which are coupled nonlinear partial differential equations. These equations were discretized in space using finite differences with 10 evenly spaced finite difference points along the column length. The spatial discretization transformed the partial differential equations into a set of ordinary differential equations, which were marched forward in time using the Runge-Kutta-Gill method (Wright, 2000). Equations 5 and 7 describing mass transfer in the particles were discretized in space using orthogonal collocation with Hermite cubic basis functions. The resulting tridiagonal matrix was solved using the Gauss-Seidel iterative method to allow rapid convergence for a large system of linear equations. The Runge-Kutta-Gill method was used to increment time intervals (Wright et al., 1998 and Wright, 2000). A total of 10 collocation points were used between the center of the particle and the surface. The collocation method is a convenient approach, since hermite cubic basis functions can be differentiated twice and still remain piecewise continuous. In particular, the collocation method was chosen for the particle-side algorithm because of its computational efficiency, which allowed for highly accurate solutions to be computed much more quickly than traditional finite difference methods (Davis, 1984). This was needed in order to resolve the moving fronts that occurred in the particles (Wright et al., 1998). The governing equations for homogeneous and pore diffusion in the fluidized-bed adsorption were solved using a simulation programmed in visual C++, version 5. All simulations were run on a Pentium II, 300-MHz personal computer.

Initially, the column was set at a specified expansion by initializing parameters obtained from tracer studies. At a specified superficial velocity, u, the expanded bed height, H, is measured. The bed void fraction, ϵ_L, was calculated as a function of the expanded bed height (McCabe et al., 1985) assuming $\epsilon_o = 0.4$ for the settled-bed void fraction. Axial dispersion coefficients, D_{ax}, at each expansion in the liquid phase were obtained by tracer studies (Wright et al., 1999; Wright, 2000). In the case presented, a step positive signal was used to obtain residence time distributions and axial dispersion coefficients were calculated from the variance, σ_θ^2, as a function of the mean residence time, t_m (Wright et al., 1999).

The algorithm depicting the flow of the computation for homogeneous or pore diffusion is shown in Figure 1. At time $t > 0$, the solution to Eqs. 1 and 2 for concentrations in the liquid phase, C, and solid phase, q', are obtained as a func-

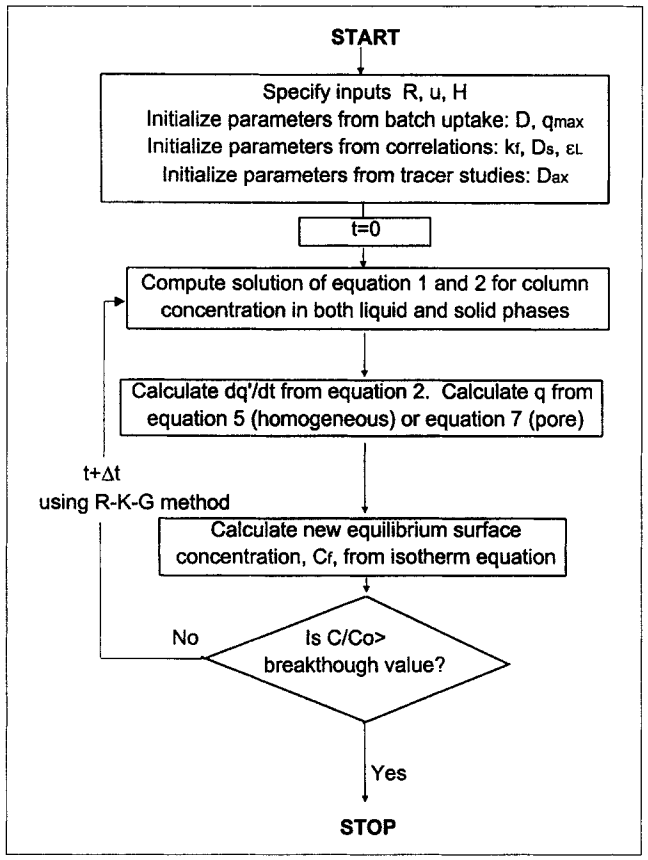

Figure 1. Algorithm for fluidized-bed adsorption simulations.

Equations 1 and 2 were discretized in space using finite differences. Equations 5 and 7 were discretized in space using orthogonal collocation with Hermite cubic basis functions. The Runge-Kutta-Gill (R-K-G) method was used to increment time intervals.

tion of axial position, taking into account liquid and solid dispersion effects. The solution to Eqs. 5 and 7 was then obtained from orthogonal collocation to calculate the solid concentration of protein in the resin as a function of axial position, q, for homogeneous and pore diffusion, respectively. Using the isotherm equation, the new equilibrium surface concentration, C_f is calculated. The simulation will continue until the value of C/Co has exceeded the preset breakthrough value. Further computational details of the numerical techniques used in the simulation are described in Wright (2000). The higher the breakthrough value of C/Co, the more steps will be required to reach convergence and computational time will increase significantly, especially for cases involving a low superficial velocity. The step size, h, was set at 0.0001 for all cases, which was small enough to ensure convergence within the accuracy required for comparison with the experimental data. In addition, decreasing the step size by half or increasing the level of spatial discretization did not lead to more than a 2% change in the breakthrough time. In addition, the computational methods were validated by solving the axial dispersion model under nonadsorbing conditions (with q and q' equal to zero), and comparing the result to the analytical solution to the dispersion model (Wehner and Wilhelm, 1956; Levenspiel, 1972; Wright, 2000).

Results and Discussion

A comparison was made of the simulation results from experimental breakthrough data for both pore diffusion and homogeneous diffusion models at each expansion. The experimental procedure and conditions are presented in Wright et al. (1999) for lysozyme adsorption on commercially available cation exchange resins with different mass-transfer mechanisms. In this work, the two chromatographic resins that were investigated (S-HyperD LS and Streamline SP) have comparable dynamic capacities for lysozyme under the same conditions in 50 mM NaOAc buffer at pH 5. The effect of increased bulk-phase viscosity by the addition of 30% glycerol was also investigated experimentally and simulated for each resin. A comparison of the experimental and simulated results was made by plotting breakthrough curves and examining breakthrough times. In addition, a quantitative assessment of the agreement between experimental and simulated breakthrough curves was made by computing a relative sum of the squares of the errors (RSSE) of the curves. The RSSE was computed as follows: $\Sigma[(e_i)^2-(e_i-s_i)^2]/(e_i)^2$, where e_i and s_i refer to experimental and simulated data points, respectively. The fractional RSSE is reported as a percentage where 100% represents perfect agreement between the curves.

Homogeneous Diffusion Using S-HyperD LS. For homogeneous diffusion, a new cation exchange resin, S-HyperD LS (BioSepra, Marlborough, MA), was used for lysozyme adsorption at $H/Ho = 2$, 3, and 4 times the settled-bed height. S-HyperD LS is a composite chromatographic resin consisting of a porous skeleton infused with a 5% cross-linked functionalized gel matrix. The unique feature of this resin is that adsorbed proteins can move between charges in the functionalized gel. Migration of the protein through the particle is random and driven by solid-phase diffusion. The homogeneous diffusion model is appropriate to describe diffusion and adsorption in S-HyperD LS, since there are no pores in the particle.

Batch adsorption studies were used to obtain the maximum dynamic capacity, q_{max}, which was 90-mg/mL resin for S-HyperD LS at equilibrium (Voute et al., 1996; Wright et al., 1998). A Malvern Mastersizer X was used to determine that the average particle radius was 78 μm, and the particle-size distribution was approximately Gaussian with skewness of 0.959 (Wright, 2000). The particle radius ranged in size from 39 μm to 156 μm. Film mass-transfer coefficients were calculated as a function of superficial velocity, bed expansion, and bulk-phase viscosity for each case using Eq. 4. The effective solid diffusion coefficient, D, for S-HyperD LS was determined to be $1.0\pm0.25\times10^{-8}$ cm^2/s (Wright et al., 1998). Model parameters obtained from tracer studies using S-HyperD LS at each expansion are provided in Table 1.

Pore Diffusion Using Streamline SP. Streamline SP (Amersham Pharmacia Biotech, Piscataway, NJ) is a macroporous cation exchange resin that has been used frequently for adsorption of proteins in numerous expanded-bed adsorption applications (Batt et al., 1995; Chang and Chase, 1996; Wnukowski and Lindgren, 1992). The resin particles are composed of a crystalline quartz core, covered by a 6% cross-linked agarose. Protein diffusion in the particle is well represented by a pore-diffusion model, taking into account

Table 1. Parameters Derived from Tracer Studies for S-HyperD LS (SHD) and Streamline SP (STR) as a Function of Superficial Velocity (u), Bed Expansion (H/Ho), and Buffer Composition (% Glycerol)

Case	Resin	Buffer (% glyc)	H/Ho	u (cm/h)	D_{ax} (m^2/s)	Re_p
A	STR	0	2	170	1.80×10^{-6}	0.121
B	STR	0	3.3	300	7.27×10^{-6}	0.185
C	SHD	0	2	300	1.78×10^{-6}	0.216
D	STR	30	2	60	1.08×10^{-6}	0.014
E	STR	30	4.5	150	6.27×10^{-6}	0.027
F	SHD	30	2	125	1.98×10^{-6}	0.031
G	SHD	30	3.05	300	7.67×10^{-6}	0.058
H	SHD	30	4	460	9.00×10^{-6}	0.076

Note: The confidence limits for H/Ho, u, D_{ax}, and Re_p are $\pm2\%$, $\pm5\%$, $\pm5\%$ and $\pm6\%$, respectively.

both solid (adsorbed) as well as pore (liquid concentration in the pores of the particle) diffusion. The effective solid diffusion coefficient for lysozyme was determined in a batch uptake system to be $3.5\pm0.5\times10^{-7}$ cm^2/s in 50 mM NaOAc buffer at pH 5. In the presence of 30% glycerol, the effective solid diffusion coefficient was determined to be $1.0\pm0.3\times10^{-7}$ cm^2/s (Wright et al., 1998).

For Streamline SP the maximum dynamic capacity at equilibrium for lysozyme was experimentally measured as 85 mg/mL. A Malvern Mastersizer X was used to determine that the average particle radius was 89 μm, with a particle-size distribution that is approximately Gaussian with skewness of 0.878 (Wright, 2000). The particle radius ranged in size from 45 to 178 μm. Film mass-transfer coefficients for Streamline SP were calculated as a function of superficial velocity, bed expansion, and bulk-phase viscosity for each case using Eq. 4. Model parameters obtained from tracer studies using Streamline SP at each expansion are provided in Table 1.

Comparison with experimental data

S-HyperD LS. The results for S-HyperD LS at bed expansions of 2, 3 and 4 times the settled-bed height showed very good agreement with experimental breakthrough data (see Figure 2). The experimental and correlation-derived parameters are given in Table 2 for each resin and condition considered in this study. In each case, breakthrough is defined at $C/Co = 0.15$ or when the exit concentration is 15% of the feedstock lysozyme solution. In most commercial applications, the adsorption would be discontinued at this point to prevent unacceptable product losses. Furthermore, since the objective of this work is to identify the main factors leading to early breakthrough in expanded-bed adsorption of proteins, we will only consider the initial portion of the breakthrough curve up to $C/Co = 0.3$.

At a bed expansion of 2 times the settled bed height, $H/Ho = 2$, the simulation output closely matched the experimental data for cases with and without 30% glycerol (see curves A and B in Figure 2). This result confirms the predictability of the simulation and validates the parameters used in the governing equations at this expansion. At a higher expansion in 30% glycerol with $H/Ho = 3$ (see curve C), the simulation showed a small discrepancy with experimental data (97.2% based on the RSSE). This deviation may be due to

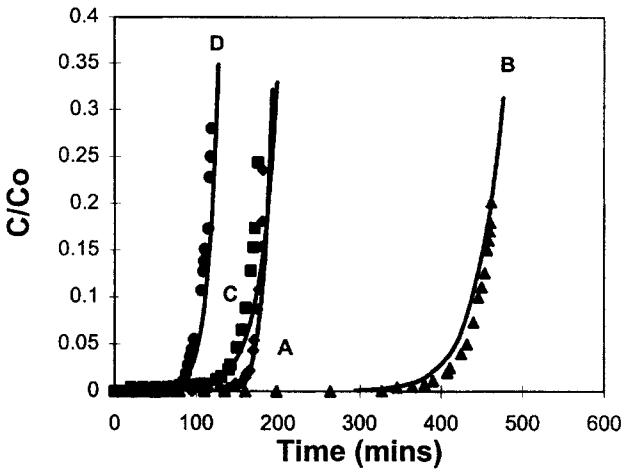

Figure 2. Experimental data (markers) vs. simulated breakthrough curves (solid lines) for S-HyperD LS.

(A) Expansion at $H/Ho = 2$ in buffer; (B) expansion at $H/Ho = 2$ in 30% glycerol; (C) expansion at $H/Ho = 3$ in glycerol; (D) expansion at $H/Ho = 4$ in 30% glycerol.

inaccuracies in the measurement of superficial velocity. Excellent agreement (99.7% based on the RSSE) was obtained when the superficial velocity was increased by 5%, which is within an acceptable range of experimental error. This result is a reasonable explanation for the deviation, considering the importance of superficial velocity in Eq. 1. At an expansion of 4 times the settled-bed height in 30% glycerol where $H/Ho = 4$, 98.8% agreement (based on the RSSE) was obtained between experimental and simulated breakthrough data (see curve D). Again it is seen that the simulation using very accurate experimental data can obtain a high degree of predictability. We believe that such close agreement between the simulation for S-HyperD LS at all expansions validates the modeling approach and suggests that the essential physics of the process have been captured in the model equations.

Streamline SP. In a similar analysis, the simulation results of Streamline SP at bed expansions of 2, 3, and 4.5 times the settled-bed height were compared to experimental data (see Figure 3). At $H/Ho = 2$, we obtained 92.8% agreement between experimental and simulated breakthrough data for the case without addition of 30% glycerol (see curve A). With addition of 30% glycerol, the agreement between experimen-

Table 2. Experimentally Derived Parameters (q/q_{max}, ϵ_L, t_m, and D) and Parameters Derived from Correlations (k_f and D_s) for Each Case in the Study

Case	q/q_{max}	ϵ_L	t_m (min)	k_f (cm/s)	D (cm^2/s)	D_s (m^2/s)
A	1	0.7	5	5.67×10^{-4}	3.50×10^{-7}	4.10×10^{-8}
B	0.75	0.82	5.4	5.81×10^{-4}	3.50×10^{-7}	1.14×10^{-7}
C	1	0.7	2.8	7.71×10^{-4}	1.00×10^{-8}	1.14×10^{-7}
D	0.86	0.7	13.1	1.51×10^{-4}	1.00×10^{-7}	6.00×10^{-9}
E	0.57	0.87	15.7	1.51×10^{-4}	1.00×10^{-7}	3.20×10^{-8}
F	1	0.7	6.1	2.18×10^{-4}	1.00×10^{-8}	2.30×10^{-8}
G	0.93	0.8	4.9	2.46×10^{-4}	1.00×10^{-8}	1.14×10^{-7}
H	0.83	0.85	4.9	4.02×10^{-4}	1.00×10^{-8}	2.47×10^{-7}

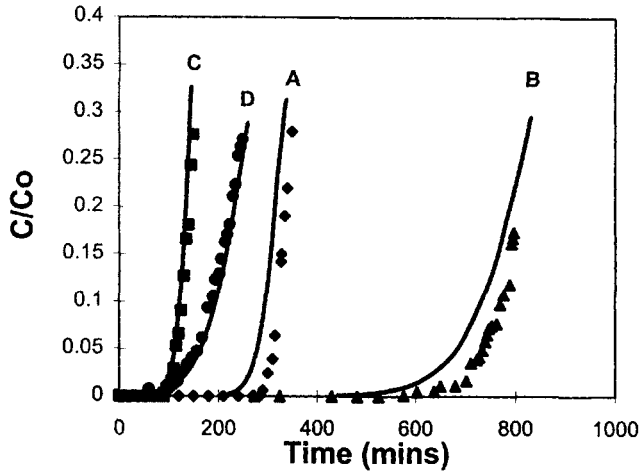

Figure 3. Experimental vs. simulated breakthrough curves for Streamline SP.

(A) Expansion at $H/Ho = 2$ in buffer; (B) expansion at $H/Ho = 2$ in 30% glycerol; (C) expansion at $H/Ho = 3$ in 30% glycerol; (D) expansion at $H/Ho = 4.5$ in 30% glycerol.

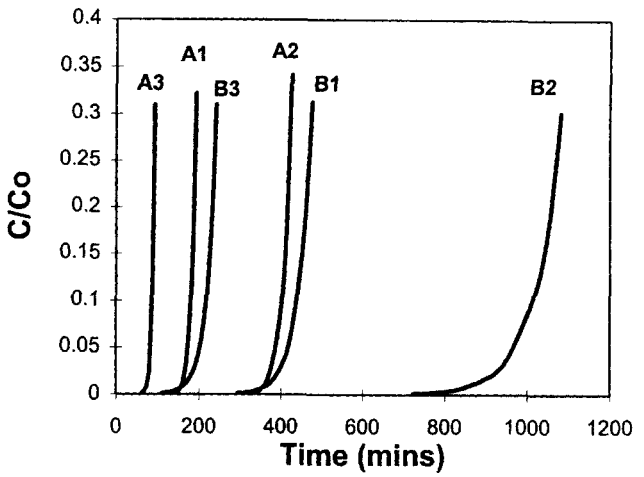

Figure 4. Homogeneous diffusion parametric analysis for the effect of superficial velocity with S-HyperD LS at $H/Ho = 2$.

(A1) Superficial velocity of 300 cm/h in buffer; (A2) superficial velocity of 150 cm/h in buffer; (A3) superficial velocity of 600 cm/h in buffer. (B1) superficial velocity of 125 cm/h in 30% glycerol; (B2) superficial velocity of 64 cm/h in 30% glycerol; (B3) superficial velocity of 250 cm/h in 30% glycerol.

tal data and simulated results was 84.5% (see curve B). As pointed out earlier, this discrepancy may be due to small inaccuracies in measurement of superficial velocity. It will be seen later that the breakthrough behavior is most sensitive to superficial velocity, and very precise measurements are required to obtain an exact match to experimental results. At $H/Ho = 3$ expansion in buffer (see curve C), we obtain agreement within 99.5%, and the breakthrough times corresponding to $C/Co = 0.15$ were nearly identical. At the highest expansion of 4.5 times the settled bed height in 30% glycerol, 99.1% agreement is obtained with experimental breakthrough data, and the times of breakthrough at $C/Co = 0.15$ were identical (see curve D).

Parametric sensitivity analysis

In order to obtain a better understanding of mass transfer and hydrodynamics in expanded-bed adsorption, a parametric sensitivity analysis of several key parameters was performed using the simulations for pore and homogeneous diffusion. The hydrodynamic parameters investigated were superficial velocity and axial dispersion. The mass-transfer parameters investigated were particle radius, film mass transfer, and effective solid diffusion coefficients. Film mass transfer is also related to the hydrodynamic parameters like bulk-phase viscosity and bed void fraction due to expansion.

Since many of the key parameters are interrelated, the individual contribution of each cannot be uncoupled in an experimental setup. A way to uncouple and study the contribution of each parameter on breakthrough behavior is through a parametric sensitivity analysis where an individual effect is changed, while the other parameters are fixed at the control case. In this study we will define the control case as the experimental conditions, since the simulation for these cases shows very good agreement for both pore and homogeneous diffusion models as a function of bed expansion and bulk-phase viscosity. Each parameter was increased and decreased by a factor of 2 to study the effect on the breakthrough curve. This range represents a realistic spread of possible operating values for each parameter.

Effect of Superficial Velocity. For homogeneous diffusion, the results of increased and decreased superficial velocity at $H/Ho = 2$ in buffer are shown in Figure 4. When the velocity is doubled, the breakthrough time is reduced to approximately half the time of the original experimental data. When the velocity is decreased by half, the breakthrough time is approximately double that of the experimental data. At the same expansion, but in 30% glycerol, a similar trend is observed, but since the bulk-phase viscosity is higher for this case, lower superficial velocities are required to attain an expansion of $H/Ho = 2$, and the breakthrough times are considerably higher. For pore diffusion, we obtained the same result, though at different breakthrough times. At expansions of $H/Ho = 2$ when the superficial velocity was doubled, the breakthrough was reduced by approximately half, and when the superficial velocity was reduced by half the breakthrough time doubled (Figure 5).

These results can be explained in terms of residence time. A shorter residence time results in a shorter amount of time for adsorption and an earlier breakthrough. Similarly, a longer residence time due to a slower superficial velocity would result in a later breakthrough. The same trend has been experimentally observed in fluidized-fiber adsorption of both lysozyme and human serum albumin (HSA) on Fractosil 1000, a macroporous resin (Finette et al., 1998). In this study, when the superficial velocity was decreased from 1.28 cm/min to 0.64 cm/min, the breakthrough time approximately doubled. When the superficial velocity increased from 1.28 cm/h to 2.55 cm/h, the breakthrough time was reduced by approximately half.

At higher expansions, the same trend is observed for homogeneous diffusion (Figure 6) and for pore diffusion (Fig-

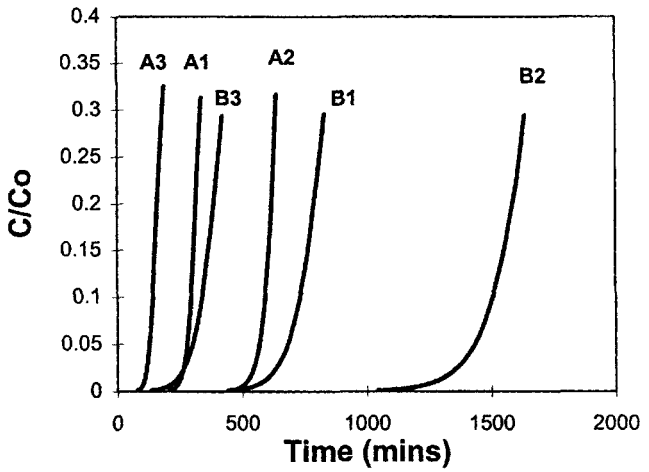

Figure 5. Pore diffusion parametric analysis on the effect of superficial velocity with Streamline SP at $H/Ho = 2$.

(A1) 170 cm/h in buffer; (A2) 85 cm/h in buffer; (A3) 340 cm/h in buffer. (B1) Sixty cm/h in 30% glycerol; (B2) 30 cm/h in 30% glycerol; (B3) 120 cm/h in 30% glycerol.

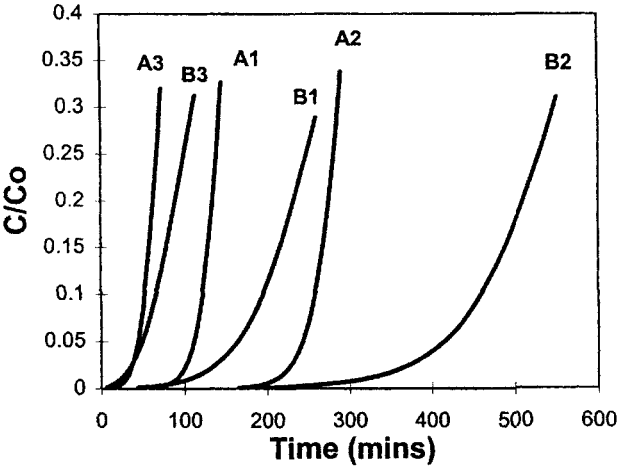

Figure 7. Pore diffusion parametric analysis on the effect of superficial velocity with Streamline SP at $H/Ho > 2$.

(A1) $H/Ho = 3$ at 300 cm/h in buffer; (A2) $H/Ho = 3$ at 150 cm/h in buffer; (A3) $H/Ho = 3$ at 600 cm/h in buffer. (B1) $H/Ho = 4.5$ at 150 cm/h in 30% glycerol; (B2) $H/Ho = 4.5$ at 75 cm/h in 30% glycerol; (B3) $H/Ho = 4.5$ at 300 cm/h in 30% glycerol.

ure 7). By doubling the linear velocity, the breakthrough time is reduced by half. When the superficial velocity is reduced by half, the residence time and breakthrough time approximately double. When all other parameters are fixed, this relationship holds for both pore diffusion and homogeneous diffusion at expansions ranging from 2 to 4.5 times the settled bed height.

To examine the effects of the mass-transfer mechanism, the resins were expanded at 300 cm/h in buffer. Since Streamline SP has a lower density than S-HyperD LS, the bed expansion for Streamline was 3 times the settled bed height compared to 2 times the settled bed height for S-HyperD LS at this superficial velocity. Under these conditions, S-HyperD LS had a breakthrough time of approximately 200 min compared to 120 min for Streamline SP. In this case it can be argued that such a comparison is biased toward S-HyperD LS at a lower expansion and lower void fraction. However, the effect of intraparticle mass-transfer resistance can be seen in Figure 8 by plotting C/Co vs. q/q_{max} for each case. If the superficial velocity is doubled for S-HyperD LS (2u SHD), and compared to the simulated mass balance for Streamline SP at 300 cm/h, breakthrough occurs when the

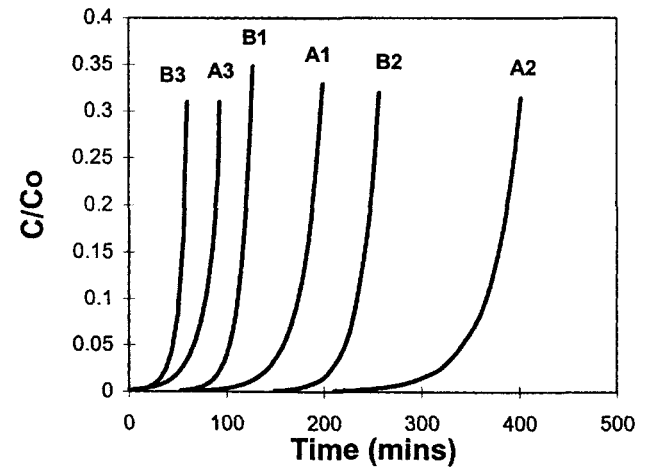

Figure 6. Homogeneous diffusion parametric analysis on the effect of superficial velocity with S-HyperD LS at $H/Ho > 2$ in 30% glycerol.

(A1) $H/Ho = 3$ at 300 cm/h; (A2) $H/Ho = 3$ at 150 cm/h; (A3) $H/Ho = 3$ at 600 cm/h. (B1) $H/Ho = 4$ at 460 cm/h; (B2) $H/Ho = 4$ at 230 cm/h; (B3) $H/Ho = 4$ at 920 cm/h.

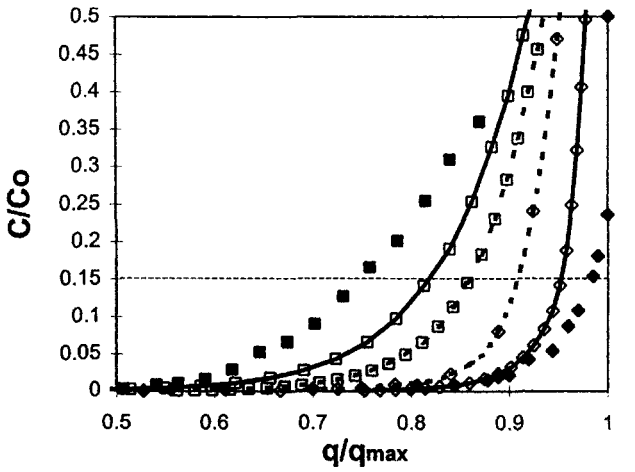

Figure 8. Mass balance for Streamline SP (STR) and S-HyperD LS (SHD) at 300 cm/h in buffer.

Effect of superficial velocity on breakthrough ($C/Co = 0.15$). ◆ SHD experimental; -◇- SHD simulation for $u = 300$ cm/h; -◇-- $2u$ SHD simulation; ■ STR experimental data; —⊟— STR simulation for $u = 300$ cm/h; –⊟– 0.5u STR simulation.

Streamline particles are approximately 80% saturated compared to 90% for S-HyperD LS particles.

Decreasing the superficial velocity for Streamline SP to 150 cm/h (0.5u STR), still does not match the breakthrough performance of S-HyperD LS. Only when the superficial velocity of S-HyperD LS is increased to 600 cm/h (2u SHD) does the performance of Streamline SP (0.5u STR) appear superior. This result suggests that intraparticle mass-transfer resistance is approximately 4 times higher for Streamline SP than for S-HyperD LS for expanded-bed adsorption in buffer. Therefore, it is possible to isolate the effect of intraparticle mass-transfer resistance by holding other parameters such as film mass transfer and axial dispersion constant and comparing uptake as a function of diffusion mechanism. We conclude that intraparticle mass-transfer resistance in expanded-bed adsorption of lysozyme is significantly lower for the homogeneous diffusion occurring in S-HyperD LS than for the macroporous diffusion occurring in Streamline SP. As a result, higher superficial velocities can be used to attain higher throughput in expanded-bed adsorption by using a high-density resin with homogeneous diffusion as the mass-transfer mechanism.

Effect of Particle Radius. The effect of mean particle radius was investigated at the low extreme of $1/2R$ (half the mean radius) and at the high extreme of $2R$ (twice the mean radius) to cover a range of particle sizes. As in the previous case, all the other parameters were held constant at the conditions used to simulate the experimental conditions. The mean particle radius for Streamline SP and S-HyperD LS were $R = 89$ μm and $R = 78$ μm, respectively. The results for expansions of two times the settled bed height are shown in Figures 9 and 10 for Streamline SP and S-HyperD LS, respectively. In buffer solution, when the particle radius was increased to $2R$, the time of breakthrough decreased for both resins. In the case of pore diffusion for Streamline SP, the breakthrough time was reduced by almost 30% relative to the

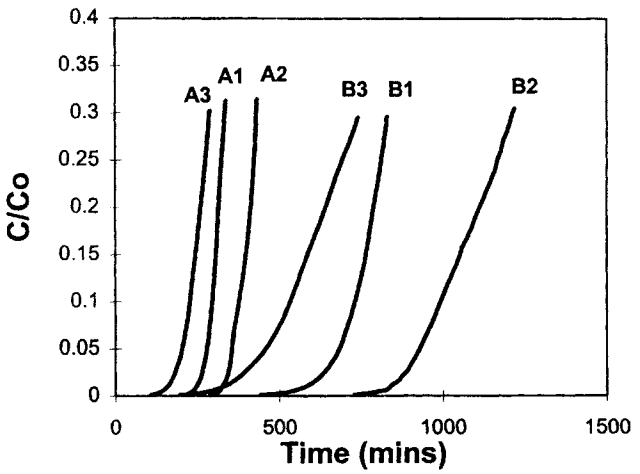

Figure 9. Pore diffusion parametric analysis on the effect of particle radius with Streamline SP at $H/Ho = 2$.

(A1) 89 μm in buffer; (A2) 45 μm in buffer; (A3) 180 μm in buffer. (B1) 89 μm in 30% glycerol; (B2) 45 μm in 30% glycerol; (B3) 180 μm in 30% glycerol.

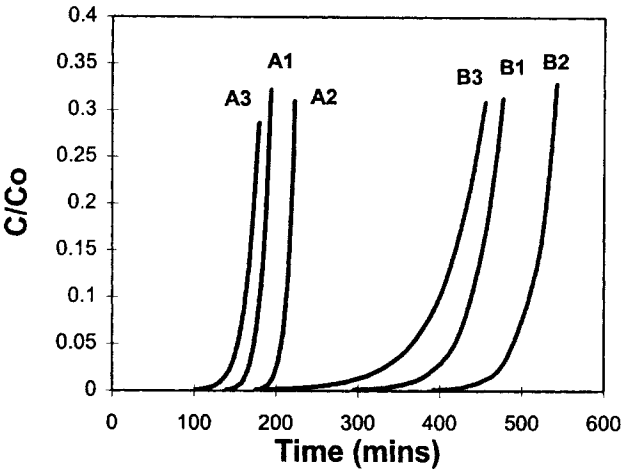

Figure 10. Homogeneous diffusion parametric analysis on the effect of particle radius with S-HyperD LS at $H/Ho = 2$.

(A1) 78 μm in buffer; (A2) 39 μm in buffer; (A3) 160 μm in buffer. (B1) 78 μm in 30% glycerol; (B2) 39 μm in 30% glycerol; (B3) 160 μm in 30% glycerol.

breakthrough time for the mean radius (of $R = 89$ μm). In the case of homogeneous diffusion for S-HyperD LS, the breakthrough time was reduced by almost 17% relative to the breakthrough time for the mean radius (of $R = 78$ μm). With glycerol, the breakthrough times were reduced by 20% and 10% for the pore and homogeneous diffusion models, respectively, at an expansion of 2 times the settled bed height. This result was expected since the superficial velocity in 30% glycerol was lower than in buffer solution at the 2X expansion. At a lower superficial velocity, the residence time increased, allowing a longer time for adsorption.

When the particle radius was decreased to $1/2R$ at two times the settled-bed height, the breakthrough time increased for both resins even though q_{max} was fixed at 90 mg/mL. This result can be explained in terms of a lower resistance to mass transfer. The effect of particle radius can be seen in the dimensionless time, $\theta = Dt/R^2$, and so the impact of particle radius can be quite significant (Wright, 2000). However, the breakthrough time was increased by 25% for pore diffusion compared to an increase of 11% for homogeneous diffusion in buffer. In glycerol at this expansion, a significant extension in the breakthrough times for each resin was observed. For pore diffusion, the breakthrough time was extended by 43% compared to an increase of 27% for homogeneous diffusion. This result is consistent with the earlier result in glycerol at $2R$. In both cases, the reduced superficial velocity due to increased bulk-phase viscosity allowed a longer residence time at the 2X expansion and breakthrough times were extended.

The effect of changes in particle radius were investigated using the simulation at expansions greater than 2 times the settled-bed height in glycerol (Figures 11 and 12). When the particle radius was doubled, the breakthrough time was decreased by 45% for the case of pore diffusion compared to a decrease of 10% for homogeneous diffusion. When the particle radius was decreased to $1/2R$, the breakthrough time increased by 23% for pore diffusion, while the increase in

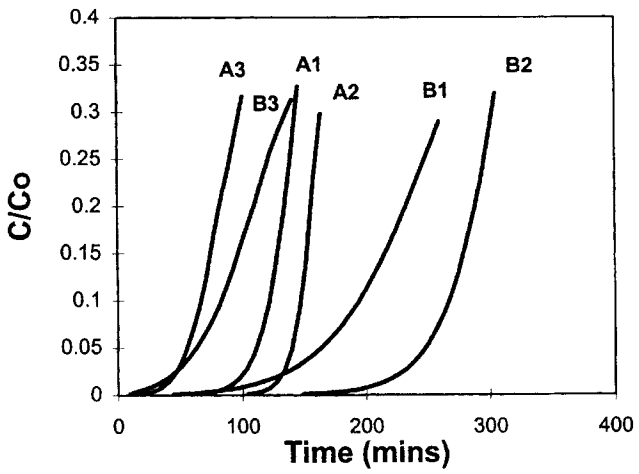

Figure 11. Pore diffusion parametric analysis on the effect of particle radius with Streamline SP at $H/Ho > 2$.

(A1) 89 μm in buffer at $H/Ho = 3$; (A2) 45 μm in buffer at $H/Ho = 3$; (A3) 180 μm in buffer at $H/Ho = 3$. (B1) 89 μm in 30% glycerol at $H/Ho = 4.5$; (B2) 45 μm in 30% glycerol at $H/Ho = 4.5$; (B3) 180 μm in 30% glycerol at $H/Ho = 4.5$.

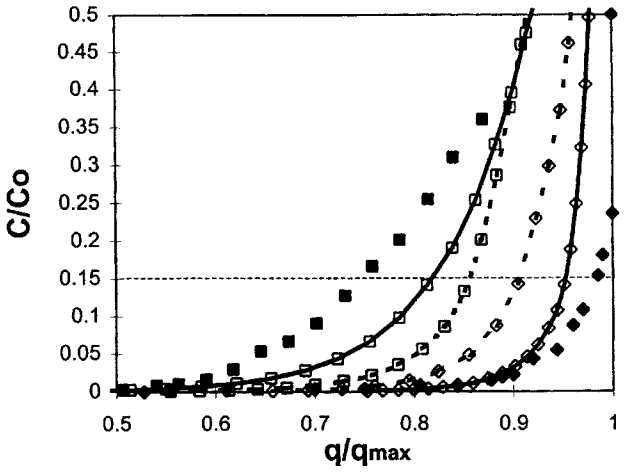

Figure 13. Mass balance for Streamline SP (STR) and S-HyperD LS (SHD) at 300 cm/h in buffer.

Effect of particle radius on breakthrough ($C/Co = 0.15$). ♦ SHD experimental data; —◇— SHD simulation for $R = 78$ μm; –◇– 2R SHD simulation: ■ STR experimental data; —⊟— STR simulation for $R = 89$ μm; –⊟– 0.5 R STR simulation.

breakthrough time for homogeneous diffusion was approximately 14%.

The simulated breakthrough results confirm those obtained experimentally in an expanded-bed adsorption system (Karau et al., 1997). By examining breakthrough behavior for small-size fractions and large-particle fractions of Streamline DEAE for BSA adsorption it was proven that breakthrough occurred later for the smallest particle diameter fraction (120–160 μm). The earliest breakthrough was obtained for the largest particle fraction (250–300 μm diameter), while the unfractionated (120–300 μm) breakthrough time was in between the high and low extremes for adsorption in macroporous particle. The experimental breakthrough results obtained by Karau et al. were explained in terms of diffusion path length or intraparticle mass-transfer resistance. Small particles have a shorter diffusion path length, and therefore less resistance than larger particles, leading to differences in breakthrough time.

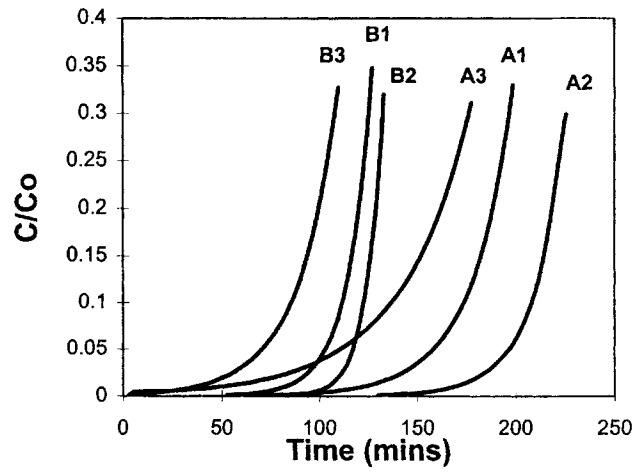

Figure 12. Homogeneous diffusion parametric analysis on the effect of particle radius with S-HyperD LS at $H/Ho > 2$ in 30% glycerol.

(A1) 78 μm at $H/Ho = 3$; (A2) 39 μm at $H/Ho = 3$; (A3) 160 μm at $H/Ho = 3$. (B1) 78 μm at $H/Ho = 4$; (B2) 39 μm at $H/Ho = 4$; (B3) 160 μm at $H/Ho = 4$.

In the simulation, the impact of changes in particle radius were most pronounced for pore diffusion, which again implies an underlying effect of intraparticle mass transfer. To study this effect we need to look at the total mass balance for increases and decreases in particle radius. To do this we will consider the case of bed expansion in buffer at a fixed superficial velocity of 300 cm/h. As stated earlier, this velocity will result in a 3X bed expansion for Streamline SP compared to a 2X expansion for S-HyperD, and the residence time for Streamline SP will be greater than that for S-HyperD. Figure 13 shows the mass balance as a function of particle radius for each resin. When the particle radius for S-HyperD is doubled to 156 μm (2R SHD), the breakthrough point decreased from 95% to approximately 85% of the maximum capacity compared to 80% for Streamline SP at 89 μm and 300 cm/h. When the particle radius for Streamline SP was reduced by half (0.5R STR), performance of Streamline SP approached that of S-HyperD. Therefore we can conclude that mass transfer by homogeneous diffusion in the S-HyperD LS has a lower intraparticle mass-transfer resistance and changes in particle radius have less impact on adsorption compared to mass transfer by pore diffusion in Streamline SP.

Effect of Axial Dispersion. It has been suggested that axial dispersion can limit performance in expanded-bed adsorption at high degrees of bed expansion at or greater than 3 times the settled-bed height, especially with an increase in viscosity (Chang and Chase, 1996). On the other hand, Thommes et al. (1995) concluded that the effect of axial dispersion decreases and dynamic capacity increases with increasing bed

Table 3. Parametric Sensitivity Analysis to Assess the Impact of Changes in D_{ax}, k_f, and D on Breakthrough Time for S-HyperD LS and Streamline SP as a Function of *H/Ho* and Bulk-Phase Viscosity

Resin and % Glycerol	H/H_o	t at C/Co = 0.15 (min)	D_{ax} (%)	k_f (%)	D (%)
Streamline SP, 0	2	308	±5	±1	±9
Streamline SP, 30	2	765	±7	±2	±4
S-HyperD LS, 0	2	195	±1	±2	±2
S-HyperD LS, 30	2	453	±2	±2	±5
Streamline SP, 0	4	116	±5	±4	±5
Streamline SP, 30	4	218	±9	±8	±30
S-HyperD LS, 30	4	183	±4	±7	±5

Note: Experimental (control) breakthrough times for each case are shown relative to the percent increase or decrease in breakthrough time due to doubling or halving each parameter.

height to column diameter. We used our simulation to test the validity of these conclusions by isolating the effect of axial dispersion at $2D_{ax}$ and $1/2$ D_{ax} as a function of mass-transfer mechanism and bed expansion for each condition. Values of axial dispersion considered in this study ranged from 0.9×10^{-6} m^2/s to 18×10^{-6} m^2/s for S-HyperD LS. For Streamline SP the range was 0.5×10^{-6} m^2/s to 15.3×10^{-6} m^2/s. The ranges of axial dispersion values compare well with those of other investigators for several fluidized-bed adsorption systems (Chang and Chase, 1996; Thommes et al., 1995; Batt et al., 1995; Wnukowski and Lindgren, 1992; Voute et al., 1996).

The results for the parametric sensitivity study to investigate D_{ax}, k_f, and D are summarized in Table 3. The corresponding breakthrough curves are presented elsewhere (Wright, 2000). For axial dispersion, it can be seen that there was very little effect on the breakthrough time for both S-HyperD LS and Streamline SP in buffer or 30% glycerol at the 2X expansion when D_{ax} was doubled or reduced by half the experimental values for these cases. Higher expansions with increased and decreased axial dispersion were also considered (Table 3). For S-HyperD LS no significant effect was observed with increases or decreases in axial dispersion at 4X expansions in 30% glycerol. For Streamline SP we observed a similar trend at the 4X expansion in buffer with a change in breakthrough time of ±5%. At 4X expansion in 30% glycerol the difference in breakthrough time increased slightly to ±9% within the breakthrough time for the control case. In all cases considered, when D_{ax} was decreased by half, the breakthrough time defined as $C/Co = 0.15$ occurred later than for cases where D_{ax} was doubled. However, the impact of changes in D_{ax} resulted in a breakthrough time that differed by less than 10% for expansions up to 4X. Therefore we can conclude that doubling the axial dispersion, even at high degrees of expansion, has almost a negligible effect on the breakthrough time.

These results are consistent with results obtained through analysis of breakthrough data as a function of the Bodenstein number, *Bo*, and it has been found that *Bo* is relatively constant as the bed height and axial dispersion is increased, even though the number of transfer units decreases (Thommes et al., 1995; Karau et al., 1997; Wright et al., 1999). The results presented here confirm that adsorption performance as a function of axial dispersion is dependent on the mass-transfer mechanism, and again we see that pore diffusion is slightly more sensitive to changes in axial dispersion than homogeneous diffusion under all conditions considered in this study. However, changes in superficial velocity and mean particle radius have a much greater impact on breakthrough time and adsorption performance than axial dispersion for both pore diffusion and homogeneous diffusion mass-transfer mechanisms.

Effect of Film Mass-Transfer Coefficient. Effects of film mass transfer can be especially difficult to quantify by traditional experimental methods, since these effects are coupled with superficial velocity and bulk-phase viscosity (Fan et al., 1960; Rowe et al., 1975; Skidmore et al., 1990). We used the simulation to isolate film mass-transfer effects from hydrodynamic effects by considering changes in breakthrough behavior at $2k_f$ and $1/2k_f$, while all other parameters were held constant at the experimentally determined values. The effect of bed expansion and mass-transfer mechanism for each case was also considered. The simulation results are presented in Table 3 for homogeneous and pore diffusion. At 2X expansion the effect on the breakthrough time with increased or decreased k_f for S-HyperD LS in buffer was almost negligible for all cases with and without addition of 30% glycerol.

The impact of changes in k_f at 4X expansion for S-HyperD LS in 30% glycerol was greater than at lower expansions (±7% compared to ±2%). This result is not unreasonable, and it has been reported that film mass-transfer effects can become quite significant when the bulk-phase viscosity is increased (Chang and Chase, 1996; Wright et al., 1998). Similar results were observed for Streamline SP in buffer and 30% glycerol at 4X expansion. The effect of doubling k_f resulted in a slight increase in breakthrough time, while decreasing k_f resulted in a shorter breakthrough time. We conclude that the effect on breakthrough behavior due to changes in k_f is essentially the same for both pore and homogeneous diffusion at all expansions, and therefore the effect of k_f on protein adsorption may be independent of diffusion mechanism in the particle. Changes in superficial velocity and mean particle radius have a greater impact on breakthrough time and adsorption performance than film mass-transfer effects.

Effect of Solid Diffusion Coefficient. Relatively little is known about the extent to which solid diffusion coefficients, D, impact expanded-bed adsorption performance. Like film mass-transfer effects, the contribution of solid diffusion coefficients are difficult to isolate from film mass transfer and hydrodynamic factors such as axial dispersion and superficial velocity. In this study, the solid diffusion coefficients for pore and homogeneous diffusion were doubled and halved to assess the impact on the breakthrough time while holding all other parameters constant. A range of 0.5×10^{-8} cm^2/s to 2×10^{8} cm^2/s for S-HyperD LS was considered, since these values are consistent with those reported by other investigators for gel-filled chromatographic media (Weaver and Carta, 1996; Voute et al., 1996). For pore diffusion, the range varied from 0.5×10^{-7} cm^2/s, to 7×10^{-7} cm^2/s, and again this range was consistent with solid-diffusion coefficients reported for porous particles (Do et al., 1982; Pedersen et al., 1985; Yoshida et al., 1994; Weaver and Carta, 1996). As in previous cases, we have investigated the effect of solid diffusion coefficients as a function of mass-transfer mechanism and degree of bed expansion.

The results of this study are shown in Table 3 for S-HyperD LS and Streamline SP in buffer and glycerol solutions at the 2X and 4X expansions. When D was changed, the breakthrough time for S-HyperD LS at the 2X expansion in buffer was changed by $\pm 2\%$ compared to the experimental data. The change in breakthrough time was only $\pm 5\%$ when D was increased or decreased for S-HyperD LS in 30% glycerol at the 2X expansion. Changes in D had a slightly more significant effect on breakthrough for Streamline SP. When D was changed, the breakthrough time varied by $\pm 9\%$ from the experimental case. In 30% glycerol, the effect was less significant at $\pm 4\%$ for Streamline SP.

At higher expansions, changes in D had a greater impact on the breakthrough time. At 4X expansion in 30% glycerol, increasing or decreasing D by a factor of 2 changed the breakthrough time $\pm 5\%$ relative to the control case for S-HyperD LS. A similar effect on breakthrough time was observed for Streamline SP at 4X expansion in buffer when D was increased or decreased. Under this condition the breakthrough time varied within $\pm 5\%$ of the control. However, at 4X expansion in 30% glycerol changes in D had an even more pronounced effect on the breakthrough time for Streamline SP. When D was changed, the breakthrough time varied by $\pm 30\%$ compared to experimental data. In each case doubling D resulted in a longer breakthrough time than when D was reduced by half. We can conclude that the contribution of solid diffusion on breakthrough behavior is dependent on mass-transfer mechanism, and the breakthrough time changes proportionally to changes in D for the pore-diffusion case, especially at high expansions with increased bulk-phase viscosity.

This result could be expected, since the values of D in buffer and 30% glycerol are different for Streamline SP. This difference is attributed to the pore concentration term, Cp, in the pore-diffusion model. Changes in bulk-phase viscosity can impact Cp and affect the total solid concentration of protein in the particle. Since homogeneous diffusion has no pores, there are no pore concentration terms, and the solid diffusion coefficient does not change as a function of bulk-phase viscosity. What is especially interesting is that the solid-diffusion coefficients for pore diffusion can have such a large impact on the shape of breakthrough curves at high degrees of bed expansion in 30% glycerol (see Wright, 2000).

This conclusion is consistent with some experimental observations for protein adsorption on Streamline XL, another type of macroporous resin for expanded-bed adsorption (Thommes, 1999). In this study it was determined that high concentrations of hIgG shifted the breakthrough curve to an early breakthrough point compared to low feed concentrations. The shape of the breakthrough curve was also changed to a more gradual slope, implying a significant contribution of solid diffusion on the overall mass-transfer process. In order to assess the impact of solid-diffusion coefficients on breakthrough curves in expanded bed adsorption, the mass-transfer mechanism of the resin must be considered.

Conclusions

In this study we have developed a simulation to account for hydrodynamic effects and mass-transfer mechanisms as a function of bed expansion in a fluidized-bed adsorption system. The simulation was validated against experimental breakthrough data using experimentally derived parameters for axial dispersion, superficial velocity, and bed height. Values for film mass transfer and solid dispersion were calculated (from experimental values of superficial velocity) using correlations. The values for solid diffusion coefficients were obtained from batch uptake simulations. For the purpose of the simulations, the resin particles were assumed to be monodisperse, and the mean particle radius was determined by Malvern analysis of each resin.

Expanded-bed adsorption results closely approximated experimental breakthrough data for both pore and homogeneous diffusion at each bed expansion within a reasonable degree of experimental error. The effect of critical parameters on breakthrough behavior was then investigated in a parametric sensitivity analysis. In this analysis, the effect of superficial velocity, particle radius, axial dispersion, film mass transfer, and effective solid-diffusion coefficient were determined at two times the experimental value and at one half the experimental value while holding all other parameters constant at the experimentally derived values.

The results of the parametric sensitivity analysis showed that superficial velocity and particle radius had the largest effects on breakthrough time. Mass-transfer mechanisms played an important role and the impact of increased or decreased superficial velocity and particle radius was more pronounced for the pore-diffusion model. The breakthrough time was decreased when the superficial velocity was doubled, and increased when the superficial velocity was reduced by half the experimental value. The net effect of increased or decreased velocity was more significant for the pore-diffusion model. Analysis of the total mass balance for S-HyperD LS and Streamline SP at 300-cm/h superficial velocity indicated that intraparticle mass-transfer resistance was approximately 4 times higher for Streamline SP. This result would explain why lysozyme adsorption in an expanded bed seemed to proceed at a slower rate with Streamline SP, even though the residence time was longer than for the cases where S-HyperD LS was studied. Similarly, effects of increased mass-transfer resistance due to increased particle radius were clearly illustrated by comparing the simulated expanded-bed adsorption performance of two resins with different mass-transfer mechanisms. At reduced particle radius and reduced intraparticle mass-transfer resistance, the breakthrough time was extended.

Secondary effects on expanded-bed adsorption were due to axial dispersion, film mass transfer, and effective solid-diffusion coefficients. Although axial dispersion effects have been reported to limit performance of expanded-bed adsorption, our parametric sensitivity analysis showed that when axial dispersion was isolated from other factors, the axial dispersion coefficient had only a small effect on breakthrough time for the range of values considered in this study. The effect of axial dispersion was more significant at high expansions for the pore-diffusion model than for the homogeneous-diffusion model, but overall the effect of axial dispersion was far less significant than the effect of superficial velocity and particle radius.

The effect of film mass transfer also showed a less significant effect on breakthrough than superficial velocity or particle radius, regardless of the mass-transfer mechanism. How-

ever, reduced values of film mass-transfer coefficients altered the shape of the breakthrough curve, especially at higher expansions in 30% glycerol. The effect of solid diffusion coefficients at low expansions had a negligible effect on the breakthrough time. At higher expansions in 30% glycerol, the contribution became quite significant, but only for the pore-diffusion model. This result can be attributed to the *Cp* terms in the pore-diffusion model. As a result, changes in the solid-phase concentration can be sensitive to changes in bulk-phase viscosity for pore diffusion.

Experimental techniques alone cannot uncouple hydrodynamic factors such as axial dispersion from mass-transfer effects, such as intraparticle mass-transfer resistance. By isolating each parameter and studying changes in the simulated breakthrough curves as a function of bed expansion and mass-transfer mechanism, we have provided a way to uncouple factors that occur simultaneously. Furthermore, the simulation can be used as a predictive tool to determine breakthrough *a priori*. All that is required are some simple batch uptake studies and tracer studies using a fluid that approximates an actual fermentation broth. For feedstocks that contain high-value therapeutic proteins, this simulation could be a valuable tool for process development and optimization with minimal risk of product loss due to unexpected breakthrough.

Acknowledgments

This work was supported by grants to B.J.G. from the New Jersey Commission on Science and Technology Particle Processing Research Center and the Charles and Johanna Biomedical Research Fund. P.R.W. is grateful to Hoffmann-La Roche, Inc., for support of this work and donation of ancillary equipment. The authors are also grateful to Amersham Pharmacia Biotech and BioSepra for donating the resins used in this work. Ronald Stickle of the Advanced Concepts Engineering Laboratory at Picatinny Arsenal is acknowledged for his expertise in visual C++ utilized in programming the expanded-bed adsorption simulations.

Notation

a_v = solid adsorption area/particle volume, cm^2/cm^3
A = cross-sectional area of the expanded-bed column, cm^2
Bo = Bodenstein number, (= uH/D_{ax})
C = bulk-phase concentration of lysozyme, mg/mL
Co = feedstock concentration of lysozyme, mg/mL
C_f = local equilibrium concentration at particle surface, mg/mL
d_p = average particle diameter, μm
D = effective solid-phase diffusion coefficient, cm^2/s
D_{ax} = axial dispersion coefficient, m^2/s
D_m = molecular diffusion coefficient of lysozyme, m^2/s
D_s = solid dispersion coefficient, cm^2/s
F = volumetric flow rate, cm^3/h
H = expanded-bed height, cm
H_o = settled-bed height, cm
H/H_o = ratio of expanded bed height to settled-bed height, dimensionless
k_f = film mass-transfer coefficient, m/s
k_a = equilibrium constant for adsorption, mg/mL/s
k_d = equilibrium constant for desorption, s^{-1}
K_s = equilibrium constant, mg/mL, (= k_d/k_a)
m = fraction available for adsorption in particle, (= $(1-\epsilon_p)/\epsilon_p$)
q = adsorbed concentration of lysozyme, mg/mL
q' = average solid-phase concentration at each collocation point, mg/mL
q_{max} = maximum adsorbed concentration of lysozyme, mg/mL
r = radial position in the particle, μm
R = particle radius, μm
Re_p = particle Reynolds number, (= $\rho_p d_p u/\mu\epsilon$)
Sc = Schmidt number, (= $\mu/\rho D_m$)
t = time, s
t_m = mean residence time, min
u = superficial linear velocity, cm/s
V_B = batch adsorption volume, mL
V_m = resin volume, mL
V = column volume, mL
z = axial position in the column, cm

Greek letters

ϵ_s = solids fraction of expanded bed
ϵ_L = liquid-phase void fraction of expanded bed
ϵ_o = settled bed porosity, (= 0.4)
ϵ_p = solid void fraction of macroporous particle
ρ = solution density, g/cm^3
ρ_p = particle density, g/cm^3
σ = variance, s
σ_θ = nondimensional variance
θ = dimensionless residence time, (= Dt/R^2)

Subscripts

p = pore concentration
s = solid-phase concentration
sm = maximum solid-phase concentration

Literature Cited

Bailey, K., K. Shriram, and M. Stocker, "Applications of Expanded Bed Adsorption in High Throughput Development of Novel Proteins," Int. Conf. on Expanded Bed Adsorption, Napa Valley, CA (1998).

Bascoul, A., J. P. Riba, C. Alran, and J. P. Couderc, "Influence of Liquid Distribution on the Axial Dispersion Coefficient in Liquid-Solid Fluidization," *Chem. Eng. J.*, **38**, 69 (1988).

Batt, B. C., V. M. Yabannavar, and V. Singh, "Expanded Bed Adsorption Process for Protein Recovery from Whole Mammalian Cell Culture Broth," *Bioseparation*, **5**, 41 (1995).

Chang, Y. K., and H. A. Chase, "Development of Operating Conditions for Protein Purification Using Expanded Bed Techniques: The Effect of the Degree of Bed Expansion on Adsorption Performance," *Biotechnol. Bioeng.*, **49**, 512 (1996).

Davis, M. E., *Numerical Methods and Modeling for Chemical Engineers*, Wiley, New York (1984).

Do, D. D., D. S. Clark, and J. E. Bailey, "Modeling Enzyme Immobilization in Porous Solid Supports," *Biotechnol. Bioeng.*, **24**, 527 (1982).

Draeger, N. M., and H. A. Chase, "Protein Adsorption in Liquid Fluidized Beds," *Institution of Chemical Engineers Symposium Series*, **18**, 161 (1990).

Draeger, N. M., and H. A. Chase, "Liquid Fluidized Beds for Protein Purification," *Trans. Inst. Chem. Eng.*, **69**(C), 45 (1991).

Fan, L. S., Y. C. Yang, and C. Y. Wen, "Mass Transfer in Semifluidized Beds for Solid-Liquid Systems," *AIChE J.*, **6**, 482 (1960).

Finette, G. M. S., Q. M. Mao, and M. T. W. Hearn, "Examination of Protein Adsorption in Fluidized Bed and Packed Bed Columns at Different Temperatures Using Frontal Chromatographic Methods," *Biotechnol. Bioeng.*, **58**, 35 (1998).

Foscolo, P. U., and L. G. Gibilaro, "A Fully Predictive Criterion for the Transition between Particulate and Aggregate Fluidization," *Chem. Eng. Sci.*, **39**, 1667 (1984).

Hall, K. R., L. C. Eagleton, A. Acrivos, and T. Vermeulen, "Pore and Solid Diffusion Kinetics in Fixed Bed Adsorption under Constant Pattern Conditions," *Ind. Eng. Chem. Fundamentals*, **5**, 212 (1966).

Johansson, B. U., and P. Wnukowski, "Hydrodynamic Stability of the Liquid Fluidized Bed of Small Particles: An Experimental Study," AIChE Meeting, Miami, FL (1992).

Karau, A., J. Benken, J. Thommes, and M. R. Kula, "The Influence of Particle Size Distribution and Operating Conditions on the Adsorption Performance in Fluidized Beds," *Biotechnol. Bioeng.*, **55**, 54 (1997).

Levenspiel, O., *Chemical Reaction Engineering*, Wiley, New York (1972).
McCabe, W. L., J. C. Smith, and P. Harriott, *Unit Operations of Chemical Engineering*, 4th ed., McGraw-Hill, New York (1985).
Pedersen, H., L. Furler, K. Venkatsubramanian, J. Prenosil, and E. Stuker, "Enzyme Adsorption in Porous Supports: Local Thermodynamic Equilibrium Model," *Biotechnol. Bioeng.*, **27**, 961 (1985).
Poncelet, D., H. Naveau, E. Nyns, and D. Dochain, "Transient Response of a Solid-Liquid Model Biological Fluidized Bed to a Step Change in Fluid Superficial Velocity," *J. of Chem. Technol. and Biotechnol.*, **48**, 439 (1990).
Richardson, J. F., and W. N. Zaki, "Sedimentation and Fluidization: Part I," *Trans. Inst. Chem. Eng.*, **32**, 35 (1954).
Rowe, P. N., "Particle to Liquid Mass Transfer in Fluidized Beds," *Chem. Eng. Sci.*, **30**, 7 (1975).
Skidmore, G. L., B. J. Horstmann, and H. A. Chase, "Modelling Single-Component Protein Adsorption to the Cation Exchanger S-Sepharose FF," *J. Chromatogr.*, **498**, 113 (1990).
Slater, M. J., *Principles of Ion Exchange Technology*, Butterworth & Heinemann, Oxford (1992).
Suzuki, M., and K. Kawazoe, "Effective Surface Diffusion Coefficients of Volatile Organic Solvents on Activated Carbon during Adsorption from Aqueous Solution," *J. Chem. Eng. Jpn.*, **8**, 379 (1975).
Thelen, T. V., and W. F. Ramirez, "Bed Height Dynamics of Expanded Beds," *Chem. Eng. Sci.*, **52**, 333 (1997).
Thelen, T. V., and W. F. Ramirez, "Modeling of Solid-Liquid Fluidization in the Stokes Flow Regime Using Two-Phase Flow Theory," *AIChE J.*, **45**, 708 (1999).
Thommes, J., M. Weiher, A. Karau, and M. R. Kula, "Hydrodynamics and Performance in Fluidized Bed Adsorption," *Biotechnol. Bioeng.*, **48**, 9 (1995).
Thommes, J., *Fluidized Bed Adsorption as a Primary Recovery Step in Protein Purification: Advances in Biochemical Engineering*, Springer-Verlag, Berlin, **58**, p. 186 (1997).
Thommes, J., "Investigations on Protein Adsorption to Agarose-Dextran Composite Media," *Biotechnol. Bioeng.*, **62**, 358 (1999).
Van Der Meer, A. P., C. M. R. J. P. Blanchard, and J. A. Wesselingh, "Mixing of Particles in Liquid Fluidized Beds," *Chem. Eng. Res. Des.*, **62**, 214 (1984).
Veeraraghavan, S., and L. T. Fan, "Modeling Adsorption in Liquid-Solid Fluidized Beds," *Chem. Eng. Sci.*, **44**, 2333 (1989).
Voute, N., P. Girot, and E. Boschetti, "HyperD: A New Ion-Exchanger for Fluidized Bed Adsorption," Int. Conf. on Expanded Bed Adsorption, Cambridge, UK (1996).
Weaver, L. E., and G. Carta, "Protein Adsorption on Cation Exchangers: Comparison of Macroporous and Gel-Composite Media," *Biotechnol. Prog.*, **12**, 342 (1996).
Wehner, J. F., and R. H. Wilhelm, "Boundary Conditions of Flow Reactor," *Chem. Eng. Sci.*, **6**, 89 (1956).
Wnukowski, P., and A. Lindgren, "Characterization of the Internal Flow Hydrodynamics in an Expanded Bed Adsorption Column," Conf. on Recovery of Biological Products VI, Interlaken, Switzerland (1992).
Wright, P. R., F. J. Muzzio, and B. J. Glasser, "Batch Uptake of Lysozyme: Effect of Solution Viscosity and Mass Transfer on Adsorption," *Biotechnol. Prog.*, **15**, 913 (1998).
Wright, P. R., F. J. Muzzio, and B. J. Glasser, "Effect of Resin Characteristics on Fluidized Bed Adsorption of Proteins," *Biotechnol. Prog.*, **15**, 932 (1999).
Wright, P. R., "The Effect of Mass Transfer and Hydrodynamics on Fluidized Bed Adsorption of Proteins," PhD Thesis, Rutgers Univ., New Brunswick, NJ (2000).
Yoshida, H., M. Yoshikama, and T. Kataoka, "Parallel Transport of BSA by Surface and Pore Diffusion in Strongly Basic Chitosan," *AIChE J.*, **40**, 2034 (1994).

Manuscript received Aug. 20, 1999, and revision received July, 2000.